EUROPEAN FUSION DEVELOPMENT AGREEMENT

JET

EFDA–JET–CP(01)02-21

R.Dux, C.Ingesson, C.Giroud, K.-D.Zastrow
and JET EFDA Contributors

Impurity Behaviour in ITB Discharges with Reversed Shear on JET

Impurity Behaviour in ITB Discharges with Reversed Shear on JET

R.Dux[1], C.Ingesson[2], C.Giroud[3], K.-D.Zastrow[4]
and JET EFDA Contributors*

[1]MPI für Plasmaphysik, EURATOM Association, D-85748 Garching, GERMANY
[2]FOM-Ri jnhuizen, Ass. EURATOM-FOM, TEC, PO BOX 1207, 3430 BE Nieuwegein, NL
[3]Association EURATOM sur la fusion, CEA Cadarache, F-13108 St Paul les Durance, FRANCE
[4]EURATOM-UKAEA Fusion Association, Culham Science Centre, Abingdon OX14 3DB, UK
** See the appendix of JET EFDA contributors (prepared by J. Paméla and E.R Solano),*
**See appendix of the paper by J.Pamela "Overview of recent JET results",*
Proceedings of the IAEA conference on Fusion Energy, Sorrento 2000

Preprint of Paper to be submitted for publication in Proceedings of the
EPS Conference,
(Maderia, Portugal 18-22 June 2001)

ABSTRACT

Impurity behaviour in scenarios with internal transport barrier is of special concern since neo-classical convection might cause strong inwardly directed drift velocities which are not suppressed by anomalous diffusion or MHD phenomena (sawteeth, fishbones etc.). The behaviour of metallic impurities in JET-discharges with an internal transport barrier (ITB) will be described in this paper.

1. ANALYSIS METHOD

Two soft X-ray (SXR) cameras with 250m thick Be filters (detection efficiency >0.1 for photons in the energy range 2.3-15keV) served as the main diagnostic tool. The SXR cameras cover the plasma cross section with 35 vertical and 17 horizontal lines-of-sight and time averaged data with a time resolution of 1ms were used. The measured radiation fluxes along the line-of-sights were unfolded by assuming constant emissivity on flux surfaces. The local emissivity $\in_{\mathrm{sxr}}$ was calculated by fitting $\in_{\mathrm{sxr}} = \exp\,[f(\rho_{\mathrm{pol}})]$ to the measured radiation fluxes where $f(\rho_{\mathrm{pol}})$ isa cubic spline and ρ_{pol} is the poloidal flux label. Poloidal variations of $\in_{\mathrm{sxr}}$ due to toroidal rotation of the plasma were not investigated since the position of the magnetic axis is not known with sufficient precision. The SXR emission was analysed to gain information about the impurity composition. The dependence of $\in_{\mathrm{sxr}}$ on the impurity density n_I and the electron density n_e can be written as

$$\in_{sxr} = \frac{n_e^2}{Z_D} L_D^{sxr} + n_e \sum_{\mathrm{I}} \mathrm{n_I} \left(L_I^{sxr} - \frac{Z_I}{Z_D} L_D^{sxr}\right). \qquad (1)$$

The first term gives the radiation for zero dilution while the second term contains the radiation caused by each impurity I including the dilution of the main ion D. For the plasma core, the mean charge Z and the total soft X-ray power coefficients L^{sxr} (including the detection efficiency of the setup) of each element can be calculated using corona ionization equilibrium and thus are mainly functions of the electron temperature T_e. The relevant atomic data were taken from the ADAS database [1], while the detection efficiency was calculated fromthe tabulated coefficients of Henke [2]. Figure 1 gives an example for the unfolding procedure for Pulse No: 53521. The high level of $\in_{\mathrm{sxr}}$ in the plasma centre can not be explained by low-Z impurities (Be, C and Ne) which mainly cause bremsstrahlung in the core. The strong emission must be due to the line radiation of metallic elements and Ni is assumed to be the predominant metallic impurity. The radiation from low-Z elements is calculated by taking the impurity densities of C and Ne (for discharges with Ne puffing) from CXRS and by increasing the C emission by 50% as an estimate for the contribution from other low-Z elements Be, N and F. Ni densities were calculated from the remaining difference $\Delta\in_{\mathrm{sxr}} = \in_{\mathrm{sxr}} - \in_{\mathrm{sxr,\ lowZ}}$. The calculation of Ni densities from $\Delta\in_{\mathrm{sxr}}$ could be checked by analysis of a discharge with Ni laser ablation. The laser ablation (LBO) caused only a negligible change of n_e and T_e and the SXR emission of Ni could be gained by taking the difference of $\in_{\mathrm{sxr}}$ after the LBO to before the LBO. About 20% of the ablated Ni particles could be found in the volume within $\rho_{\mathrm{pol}} = 0.75$ which is in agreement with the expected penetration of Ni.

2. ITB DISCHARGES WITH HIGH PERFORMANCE

Figure 2 gives the evolution of the impurity densities in the reversed shear Pulse No: 51976 with a high performance ITB of 1 s duration. The toroidal field is B_T = 3.4T and during the high power phase of the discharge, the rising plasma current has an average value of I_p = 2.2MA. The application of Lower Hybrid Current Drive(LHCD) during the current ramp phase results in a reversed shear current profile at the time of the application of the main heating power. During the high power phase (t>5s) the plasma is constantly heated with 17MW of NBI and 4MW of RF. A strong barrier in T_i, T_e and n_e forms at t ≈ 5.9s [3]. The total neutron rate reaches a maximum value of $4.1\times10^{16}s^{-1}$. A constant Ne puff is applied for t>4s. The profile evolution of T_i, n_e and the densities of C, Ne and Ni is shown for four time slices. Before the formation of the strong barrier, at t = 5.8s, T_i shows an almost constant gradient length, and the impurity density profile is hollow or mildly peaked. At t = 6.2s, the normalized T_i gradient is increased at a mid plane radius of R ≈ 3.5m. The radius with the increased normalized T_i gradient shifts towards larger radii for the following time slices at t = 6.6s and t = 6.8s. This movement is due to the expansion of the barrier location and to the increasing Shavranov shift. For the later times, the radial region of the T_i barrier location is depicted by the vertical light grey bar. Inside that region T_i becomes progressively flat. Here, n_e and the impurity densities develop the strongest gradient. The radial region with increased gradient of the densities is given by a darker grey bar in Fig. 2. The impurity peaking increases with the impurity charge Z and is weakest for C and strongest for Ni. The central Z_{eff} is dominated by Ni and reaches a value of Z_{eff} = 3.5 for t = 6.9s. In equilibrium, the radial gradient of the density n at radius r (impurity or electron density) depends on the ratio of the radial drift velocity υ, the diffusion coefficient D at this radius and the source Q inside r.

$$\frac{1}{n^{eq}}\frac{dn^{eq}}{dr} = \frac{\upsilon}{D} - \frac{1}{Dn^{eq}r}\int_0^r Qrdr. \quad (2)$$

For the electron density profile, both terms have to be considered since there are central electron sources due to the neutral beam fueling. For the impurity densities, however, the source is located in the scrape of layer and the peaking of the impurity densities is given by the ratio υ / D. Neo-classical transport parameters of standard neo-classical theory were numerically evaluated with STRAHL/NEOART [4,5]. For impurity I, the neo-classical diffusion coefficient D^I_{neo} and drift velocity υ^I_{neo} have the form

$$D^I_{neo} = \sum_X \sum_J D^X_{IJ} \qquad \upsilon^I_{neo} = \sum_X \sum_J (c^{n,X}_{IJ} \frac{1}{n_J}\frac{dn_J}{dr} + c^{T,X}_{IJ}\frac{1}{n_J}\frac{dT_J}{dr}), \quad (3)$$

where the summation over J includes all species J ≠ I and the summation over X shall denote the classical, banana-plateau and Pfirsch-Schlüter contribution. The coefficients in υ_{neo} are proportional to the diffusion coefficient of each contribution times the impurity charge: $c^X_{IJ} \propto D^X_{IJ} Z_I/Z_J$. If the weight of the different contributions does not change too much with Z_I, υ_{neo} is almost proportional to $Z_I D_{neo}$. The density gradient terms in the equation for υ_{neo} drive inwardly directed convective fluxes, while the temperature gradients yield outwardly directed drift velocities. In Fig.3a, the collision frequencies of Ni with D, C, Ne and Ni are shown for Pulse No: 51976 at t = 6.6 s. The collisions of Ni with C and Ne are as frequent as the collisions with D and had to be considered in the neo-classical calculation. The required gradients of the densities and of T_i were taken from the experiment as shown in Fig.2, where the deuterium density follows from n_e, the impurity densities and quasi neutrality. Equal temperature of all ion species was assumed. In Fig.3b the calculated radial profile of υ_{neo} / D_{neo} is depicted for C, Ne and Ni. Close to the axis (R≤3.35m) the poloidal field becomes very low, the orbits of trapped particles are very large and standard neo-classical theory may not be applied. In the region with weaker temperature gradient and pronounced electron peaking (dark grey bar in Fig.3b and 2), the neo-classical transport is strongly convective with inwardly directed (negative) drift velocities . The absolute value of υ_{neo} / D_{neo} rises with Z as experimentally observed. In the region with the strong temperature gradient (light grey bar in Fig.3b and 2) the drift term is close to zero or becomes outwardly directed for the case of Ni. Thus the impurity behaviour can be understood in terms of neo-classical transport, where the drift velocities are governed by the ratio of the temperature to the density gradient. The calculated values of υ_{neo}, however, have a high uncertainty due to the uncertainty of all the gradients which enter into eq.(3) and the comparison is thus more qualitative.

3. LONG ITB DISCHARGES

In Fig.4 two reversed shear Pulses (No: 53521 in black, No: 53697 in grey) with long ITB phases are compared. The toroidal field is B_T = 3.4T. During the shown time interval, the plasma current has a constant value of I_p = 2MA for Pulse No: 53521 and I_p = 1.8MA for Pulse No: 53697 and in both discharges the plasma is heated with ≈ 15MW of NBI and 3-4MW of RF. LHCD is applied throughout the discharges. The total neutron rate is in the range $1.0\text{-}1.4\times10^{16}s^{-1}$. In Pulse No: 53521, the ITB in the ion channel is sustained for 27 confinement times [6]. The temperatures T_i and T_e and the Ni density n_{Ni} close to the plasma centre and at half radius are shown. Two horizontal interferrometer channels (central, and half radius) give the evolution of the electron density profile. T_e and T_i are similar in both discharges with somewhat stronger gradients in Pulse No: 53521. The electron density, however, shows a pronounced difference and evolves a stronger peaking in Pulse No: 53521, where n_{Ni} becomes extremely peaked. The correlation between density peaking and Ni peaking can be understood in terms of neo-classical transport as discussed in the previous section. For Pulse No: 53521 at t ≈10.7s, the accumulated Ni is the dominant Z_{eff} contributor with central Z_{eff} = 7 and the dilution due to Ni is $\Delta n_e / n_e$ = 20%. The central SXR emission $\epsilon_{sxr} = 0.6\times10^5$ Wm^{-3} (see Fig.1) corresponds to a calculated local radiation loss of $\epsilon = 1.4\times10^5$ Wm^{-3}, which is about the central heating power density into the electrons. Thus, the loss of confinement at t = 11.1s, which is very strong in the Ni channel, is probably a radiative collapse. MHD events, which lead to a sawtooth like signature of T_e, correlate with a decrease of the Ni peaking, which might become very strong as for Pulse No: 53697 at t = 10.1s, where the central radiation is too low to explain a radiative collapse. Here, a n = 1-mode is observed, followed by a decrease of central plasma rotation by ≈ 30%, central particle density is lost and the Ni profile becomes flat. Further investigation is needed for these phenomena. Carbon density profiles from CXRS peak only slightly stronger as n_e and the concentration of C stays almost constant resembling the same Z dependence of impurity transport as in Pulse No: 51976.

CONCLUSION

In ITB discharges with reversed shear, metallic impurities accumulate in cases with too strong peaking of the density profile. The peaking increases with the impurity charge and is low for the low-Z elements C and Ne. This behaviour is in agreement with neo-classical convection.

REFERENCES

[1]. H.P.Summers, Jet-IR 06, Jet Joint Undertaking, Culham (1994).

[2]. http://xray.uu.se/hypertext/henke.html.

[3]. C.Chalis, et al, this conference.

[4]. R.Dux, A.G.Peeters, et al., Nucl. Fusion **40** (2000) 1721.

[5]. S.P.Hirshman, Sigmar, D.J., Nucl. Fusion **21** (1981) 1079.

[6]. A.Becoulet, et al this conference.

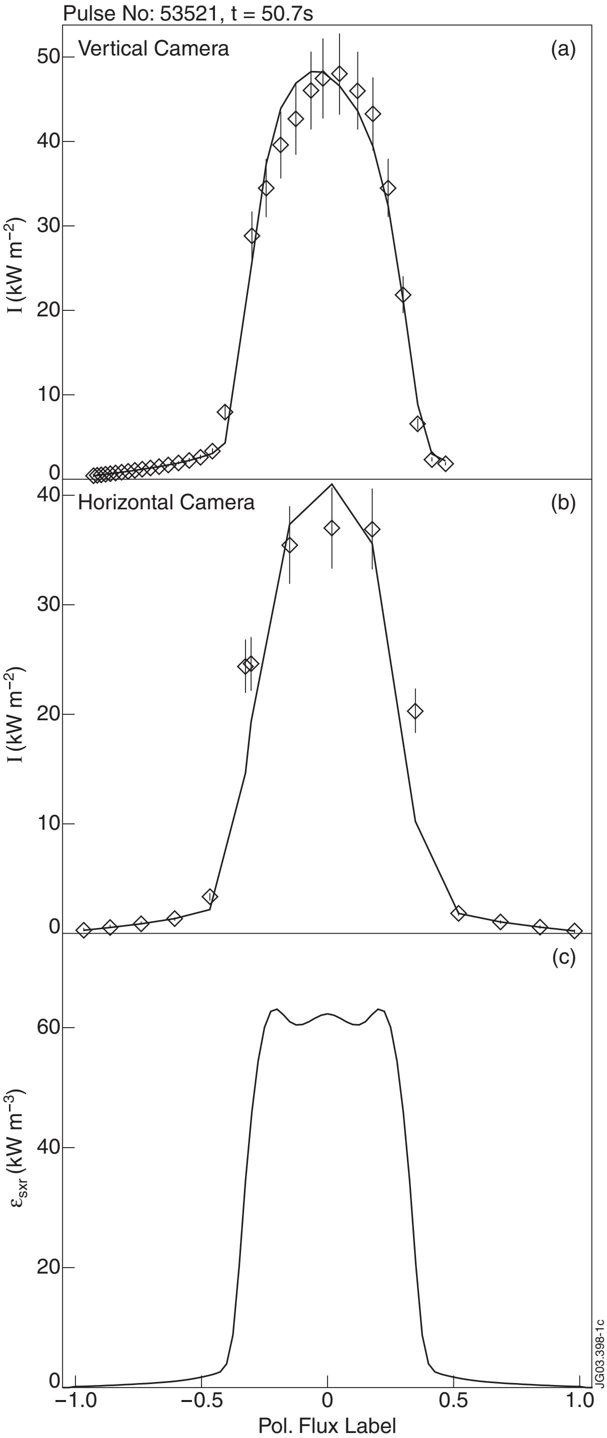

Figure 1: Measured radiation fluxes for two SXR cameras (a,b) and fitted local emissivity(c) for Pulse No: 53521 at t = 10.7s. Calculated radiation fluxes from the fit are shown as a solid line (a,b).

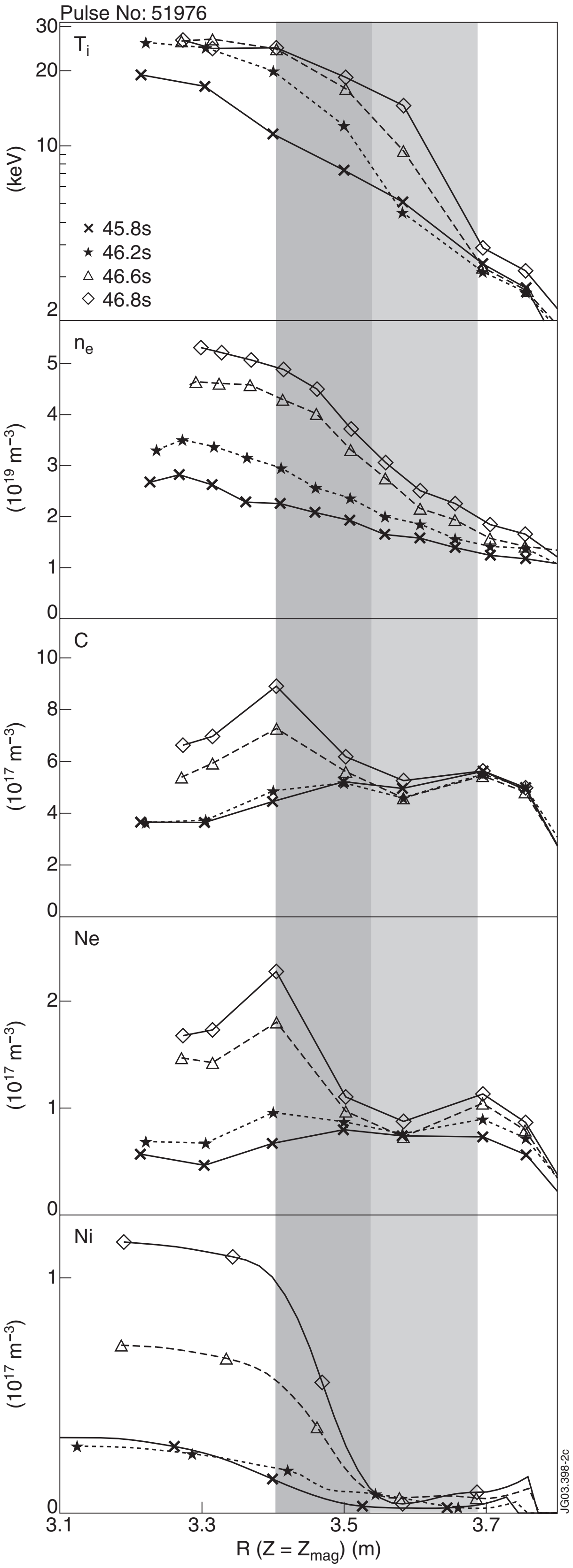

Figure 2: Evolution of the radial profiles of T_i, n_e, n_C, n_{Ne} and n_{Ni} or the Pulse No: 51976.

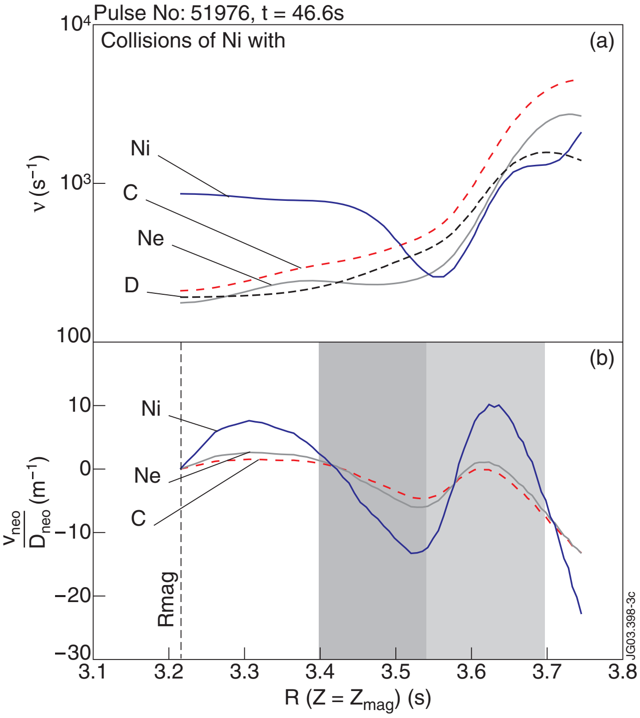

Figure 3: Radial profile for the collision frequencies of Ni and the ratio υ_{neo}/D_{neo} for C, Ne and Ni in Pulse No: 51976 at = 6.6s.

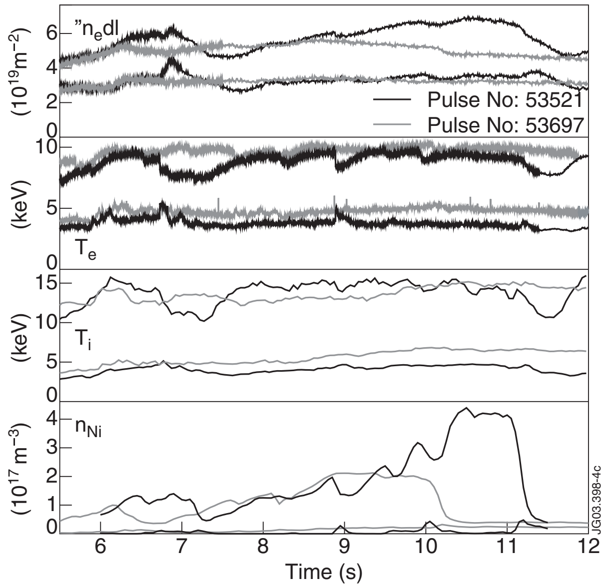

Figure 4: Time traces for $\int n_e dl$, T_e, T_i and n_{Ni} for two reversed shear Pulses No.s (53521 in black, 53697 in grey) with long ITB phases are compared.